MODELLING AND SIMULATION OF BIFURCATION DYNAMICS OF SPATIAL DOUBLE PENDULUM WITH RIGID LIMITER OF MOTION

Awrejcewicz, J., Kudra, G.

Lodz University of Technology, Department of Automation, Biomechanics and Mechatronics
Stefanowski St. 1/15, 90-924 Lodz, Poland
grzegorz.kudra@p.lodz.pl

ABSTRACT
The purpose of this work is to present mathematical model of a spatial double pendulum with rigid movable obstacle and report results of numerical simulations with particular emphasis on specific bifurcation phenomena as well as effectiveness and importance (influence on system dynamics) of individual elements of specific (reduced) model of contact forces. The system consists of two links connected to each other and suspended (by the use of two universal joints) on the shaft performing rotational motion about its horizontal axis according to a given function of time (kinematic driving). The second link ends with a ball which can come into contact (impacts and permanent contact) with a planar and rotating obstacle situated below the pendulum. In this work we use and expand our earlier developed models of contact forces (resulting friction force and rolling resistance). The models of friction force and moment are based on the integral model developed under assumption of fully developed sliding on a planar contact area, where at each point the classical Coulomb's friction law is valid. The integral models are then replaced by special approximations being more suitable for fast numerical simulations. In the present work we model impacts with non-point frictional contacts assuming Hertzian compliance of the obstacle. The developed models as well as the planned experimental setup allow us for testing importance of its individual elements and may lead to general conclusions concerning modelling and effective numerical simulations of mechanical systems with frictional contacts.

KEYWORDS: dry friction, impacts, mathematical modelling, bifurcation, model reduction

1. INTRODUCTION

Pendulum and multi-pendulum mechanical systems play a very important role as a paradigm of many problems of pure nonlinear dynamics, as well as technical questions encountered in mechanical engineering, biomechanics, control theory and mechatronics. Among them one can indicate the systems of spatial pendulums, for which one can easy find works concerning single spherical pendulum and its different configurations like single rigid body model [1-3] or mathematical spherical pendulum [4]. Spatial multi-pendulum systems are much more difficult to find as an object of scientific analysis concerning pure non-linear dynamics [5].
On the other hand, impact and friction are common phenomena in mechanical engineering systems. They are a subject of interest as elements changing drastically bifurcation dynamics of mechanical systems, leading to new kinds of bifurcations and requiring new methods of analysis. Another area of interest related to impacts and friction is that of developing new models and methods leading to fast and realistic numerical simulations of such kind of systems.
One of the problems being the base for modelling impact in 3D space is that of resulting friction forces appearing on finite area contact. Instead of solving the full contact problem, which numerical solution requires however a lot of computational power, one can try to find some kind of simplified or reduced models. An integral model of friction force for fully developed sliding on circular contact area and Coulomb friction law was presented in the work of Contensou [6]. In order to avoid necessity of integration over the contact area, another group of researchers developed special group of approximations of the integral model of friction [7, 8], also for

other than circular shapes of the contact [9]. The results were then applied to modelling and numerical simulations of the wobblestone [10], billiard ball and full ellipsoid of revolution [11, 12].
The present work joins and continues studies of the works [5, 9-12]. The double spatial pendulum is equipped with a ball at the end of the second pendulum, which can come into a contact with rotating obstacle. The friction force is modelled based on the works [9-12], while normal force is modelled using Hertz stiffness with damping [13, 14].

2. MATHEMATICAL MODEL

Figure 1 exhibits the physical concept of the investigated system. There is defined the global (fixed) reference frame O_1xyz with the origin at the point O_1, which is the geometric center of the first massless Cardan-Hook joint (intersection of its two axes) connecting two bodies: body 0 and the first link 1 of mass m_1. The rotor performs rotational motion about the axis O_1x and its angular position is described by angle ψ_1. Introducing the coordinate system $O_1x_1y_1z_1$ fixed with respect to the body 1, one can describe the angular position of the link 1 by the following sequence of rotations: by angle ψ_1 about axis x_{11}, by angle θ_1 about axis x_{12} and by angle φ_1 about axis x_{13} (assuming that for $\psi_1= \theta_1= \varphi_1=0$ the two coordinate systems $O_1x_1y_1z_1$ and O_1xyz overlap each other). The center O_2 of the next massless Cardan-Hook joint, connecting the link 1 with the body 2 of mass m_2, lies on the axis O_1z_1 and its position is defined by the parameter $L_1= O_1O_2$. Angular position of the link 2 is then described by the following sequence of rotations: by angle θ_2 about axis y_2 and by angle φ_2 about axis z_2, where we have assumed the coordinate system $O_2x_2y_2z_2$, originated at the point O_2 and, for $\theta_2= \varphi_2=0$, of axes parallel to the corresponding ones of the system $O_1x_1y_1z_1$.

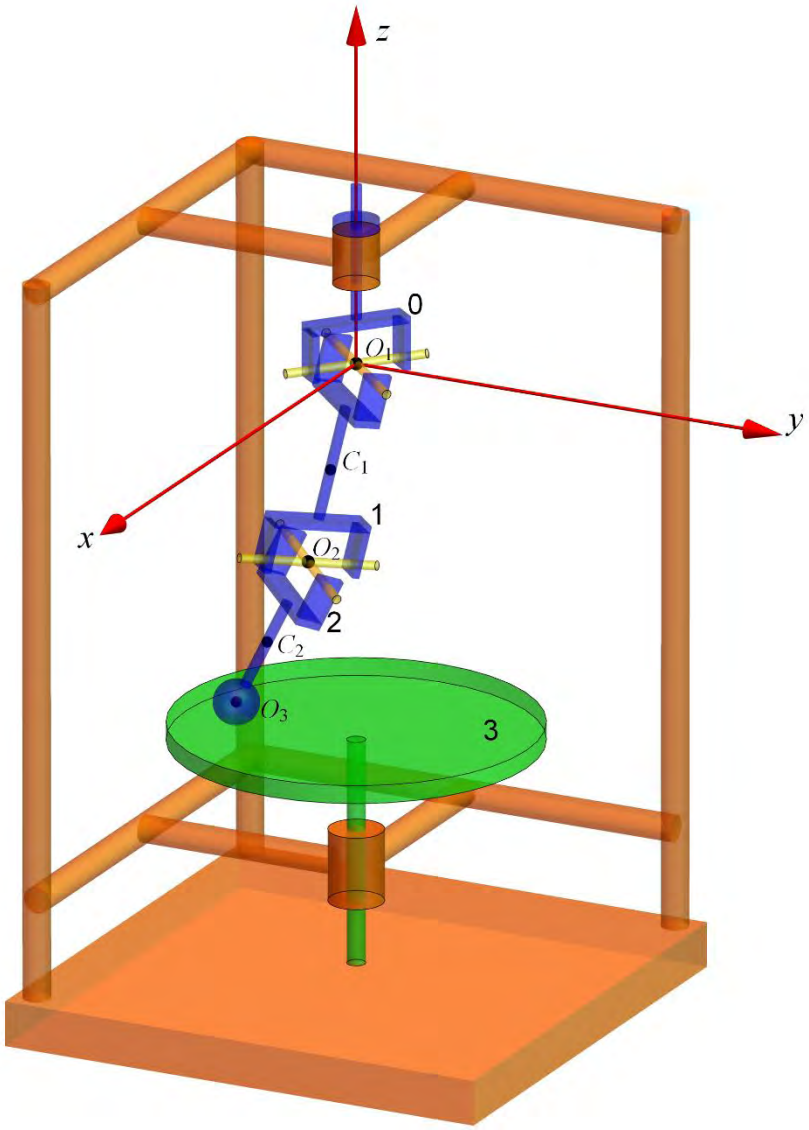

Figure 1 – The coupled pendulum with obstacle.

The second link ends with a ball of radius R_b and centered at the point O_3 lying on the axis O_2x_{13} and with position described by the parameter $L_2= O_2O_3$. It is assumed that the mass centers C_1 and C_2 of both pendulums lie on the corresponding axes O_1z_1 or O_2z_2 and their positions are defined by the parameters $e_1= O_1C_1$ and $e_2= O_2C_2$. Moreover the axes of the coordinate systems $O_1x_1y_1z_1$ and $O_2x_2y_2z_2$ are the principal axes of inertia of the corresponding bodies, thus their mass distributions are defined by six parameters I_{xi}, I_{yi} and I_{zi}, denoting the corresponding principal central moments of inertia of the link number i (i=1,2) with respect to the axis parallel to the corresponding axis O_ix_i, O_iy_i or O_iz_i. The ball ending the second pendulum can come into a contact with the obstacle 3 having the form of disk rotating with velocity ω_d about the axis z of the global coordinate system and having also possibility of motion along its horizontal axis – the corresponding position is defined by the parameter z_0 describing the coordinate of any point of the disk's surface along the axis z. All the bodies are assumed to be rigid.

The introduced above definitions result in the following transformation rules between the vector's coordinates expressed in the corresponding coordinate systems:

$$\begin{bmatrix} u_x & u_y & u_z \end{bmatrix}^T = \mathbf{A}_1 \begin{bmatrix} u_{x_1} & u_{y_1} & u_{z_1} \end{bmatrix}^T,$$
$$\begin{bmatrix} u_{x_1} & u_{y_1} & u_{z_1} \end{bmatrix}^T = \mathbf{A}_2 \begin{bmatrix} u_{x_2} & u_{y_2} & u_{z_2} \end{bmatrix}^T, \tag{1}$$

where

$$\mathbf{A}_1 = \mathbf{A}_{11}\mathbf{A}_{12}\mathbf{A}_{13}, \qquad \mathbf{A}_2 = \mathbf{A}_{22}\mathbf{A}_{23},$$

$$\mathbf{A}_{11} = \begin{bmatrix} \cos\psi_1 & -\sin\psi_1 & 0 \\ \sin\psi_1 & \cos\psi_1 & 0 \\ 0 & 0 & 1 \end{bmatrix}, \quad \mathbf{A}_{12} = \begin{bmatrix} 1 & 0 & 0 \\ 0 & \cos\theta_1 & -\sin\theta_1 \\ 0 & \sin\theta_1 & \cos\theta_1 \end{bmatrix}, \quad \mathbf{A}_{13} = \begin{bmatrix} \cos\varphi_1 & 0 & \sin\varphi_1 \\ 0 & 1 & 0 \\ -\sin\varphi_1 & 0 & \cos\varphi_1 \end{bmatrix}, \tag{2}$$

$$\mathbf{A}_{22} = \begin{bmatrix} 1 & 0 & 0 \\ 0 & \cos\theta_2 & -\sin\theta_2 \\ 0 & \sin\theta_2 & \cos\theta_2 \end{bmatrix}, \quad \mathbf{A}_{23} = \begin{bmatrix} \cos\varphi_2 & 0 & \sin\varphi_2 \\ 0 & 1 & 0 \\ -\sin\varphi_2 & 0 & \cos\varphi_2 \end{bmatrix},$$

and where u_ξ is component of a vector $\mathbf{u}$ along axis ξ.

The angular position of the body 1 (see Fig. 1) is assumed as the following function of time (kinematic driving):

$$\psi_1(t) = \omega_0 t + \frac{q}{\Omega}\sin(\Omega t) + \psi_{10}, \tag{3}$$

which results in the angular velocity of driving $\omega(t) = \omega_0 + q\cos(\Omega t)$ and where ω_o, q, Ω and ψ_{10} are constant parameters representing constant component and amplitude of angular velocity, the corresponding frequency and initial angular position of the body 0, respectively.

The governing equations of motion are expressed using the Lagrange's formalism:

$$\frac{d}{dt}\left(\frac{\partial T}{\partial \dot{\theta}_i}\right) - \frac{\partial T}{\partial \theta_i} + \frac{\partial V}{\partial \theta_i} = Q_{\theta_i}, \quad \frac{d}{dt}\left(\frac{\partial T}{\partial \dot{\varphi}_i}\right) - \frac{\partial T}{\partial \varphi_i} + \frac{\partial V}{\partial \varphi_i} = Q_{\varphi_i}, \quad i=1, 2 \tag{4}$$

where T - is kinetic energy, V - potential energy of gravity forces, Q_{θ_i} and Q_{φ_i} - are the corresponding generalized forces, which are expressed in the following way

$$Q_{\theta_i} = Q_{\theta_i c} - Q_{\theta_i b}, \quad Q_{\varphi i} = Q_{\varphi_i c} - Q_{\varphi_i b} \quad i=1, 2 \tag{5}$$

where $Q_{\theta_i c}$ and $Q_{\varphi_i c}$ are their components related to contact forces (between the pendulum's ball and disk 3), while $Q_{\theta_i c}$ and $Q_{\varphi_i c}$ represent damping in the joints.

Model of damping in the joints, taking into account future experiments and present experience of the authors, is assumed to have the following nonlinear form:

$$Q_{\theta_i b} = M_b \frac{\dot{\theta}_i}{\sqrt{\dot{\theta}_i^2 + \varepsilon_b^2}}, \quad Q_{\varphi_i b} = M_b \frac{\dot{\varphi}_i}{\sqrt{\dot{\varphi}_i^2 + \varepsilon_b^2}}, \quad i=1, 2 \tag{6}$$

where M_b and ε_b are constant parameters common for all the joints.

The generalized contact forces are computed in the following way

$$Q_{\theta_i c} = \mathbf{F}_c \cdot \frac{\partial \mathbf{r}_{A_2}}{\partial \theta_i}, \quad Q_{\varphi_i c} = \mathbf{F}_c \cdot \frac{\partial \mathbf{r}_{A_2}}{\partial \varphi_i}, \quad i=1, 2 \tag{7}$$

where $\mathbf{F}_c$ is resultant contact force acting on the ball of the second link at the contact point A and A_2 is the body 2 fixed point instantaneously taking the position of the point A. The contact force consists of two components

$$\mathbf{F}_c = \mathbf{N} + \mathbf{T} \tag{8}$$

where $\mathbf{N}$ is normal component of reaction and $\mathbf{T}$ is resultant friction force reduced to the point A.

The normal component is modelled as

$$\mathbf{N} = N\,\mathbf{n}, \tag{9}$$

where $\mathbf{n}$ is unit vector normal to the disk's 3 surface and directed upward N is expressed in the following way [13,14]

$$N = |h|^{3/2} k\left(1 + b\dot{h}\right)\mathbf{1}(-h), \tag{10}$$

where h is distance between the ball and the obstacle. It is assumed that the bodies 2 and 3 can penetrate each other and negative h stands for depth of this penetration. Then the point of the contact A is defined as the point lying on the surface of the ball for which h reach the minimum value. In the formula (10) k stands for stiffness of the contact, b is damping coefficient and $\mathbf{1}$ is unit step function. The presented model of stiffness is based on the stiffness of the Hertz contact, where for the contact of a ball of radius R_k with an elastic semispace

$$k = \frac{4\sqrt{R_b}}{3\left(\frac{1-\nu_1}{E_1} + \frac{1-\nu_2}{E_2}\right)}, \tag{11}$$

and where ν_1 and ν_2 are Poisson's coefficients of materials of the contacting bodies, while E_1 and E_2 are their Young's modulus.

Friction force is modelled based on the previous works of the authors [9-12]

$$\mathbf{T} = -\mu N \frac{\mathbf{v}_s}{\sqrt{\mathbf{v}_s^2 + b_T^2 a_r^2 \boldsymbol{\omega}_s^2 + \varepsilon^2}}, \tag{12}$$

where μ is friction coefficient, b_t, ε – constant parameters, a_r – radius of the corresponding hertzian contact, while $\mathbf{v}_s$ and $\boldsymbol{\omega}_s$ are relative linear and angular sliding velocities at the point of the contact

$$\mathbf{v}_s = \mathbf{v}_{A_2 t} - \mathbf{v}_{A_3}\,,\ \boldsymbol{\omega}_s = \boldsymbol{\omega}_{2n} - \boldsymbol{\omega}_3 \tag{13}$$

where $\mathbf{v}_{A_2 t}$ - is component of velocity of the point A_2 (body 2 fixed point) tangent to the surface of the obstacle, $\mathbf{v}_{A_3}$ – velocity of the point A_3 (point of the obstacle instantaneously taking the position of the point A), $\boldsymbol{\omega}_{2n}$ – component of angular velocity of the body 2 normal to the disk 3, $\boldsymbol{\omega}_3$ – angular velocity of obstacle. The size of the contact is calculated according to the following formula

$$a_r = \left(\frac{3}{4} N \left(\frac{1-\nu_1}{E_1} + \frac{1-\nu_2}{E_2} \right) R_b \right)^{\frac{1}{3}}. \tag{14}$$

Figure 2 exhibits test of the model (10, 11) of stiffness and damping of the obstacle. It is considered a ball of mass m falling and bouncing perpendicularly onto a horizontal plane

$$\ddot{x} + g + \frac{k}{m} x^{3/2} \left(1 + b\dot{x}\right) \mathbf{1}(-x) = 0\,, \tag{15}$$

where g=9.81 m/s^2 is gravitational acceleration. The remaining parameters are assumed as: R_b=0.025 m, $\nu_1 = \nu_2$= 0.3, $E_1 = E_2 = 2 \cdot 10^9$ N/m^2, b = 0.5 m^{-1}s. The results presented in Fig. 2 indicate, that the assumed value of daming coefficent b is resonable. Our tests (not shown here) indicate, that the ball's behavior seems not to depent noticable on the coefficient k/m.

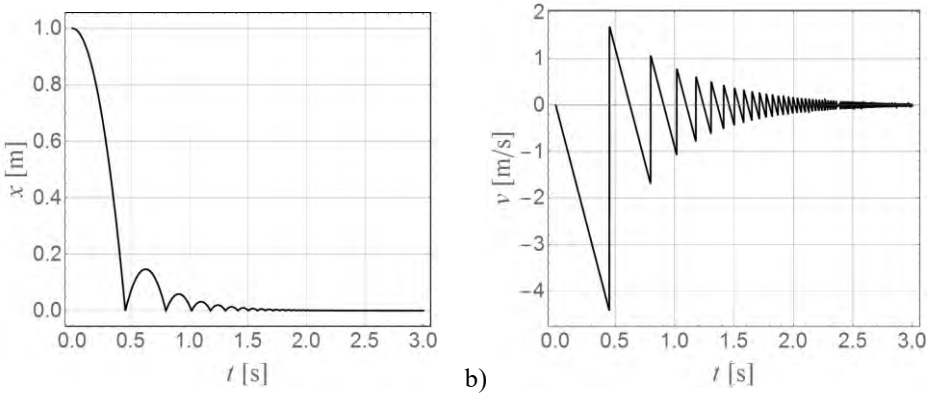

a) b)

Figure 2. Position x (a) and velocity v (b) of a ball falling perpendicularly onto a horizontal plane for the following parameters: m=0.5 kg, g=9.81 m/s^2, R_b=0.025 m, $\nu_1 = \nu_2$= 0.3, $E_1 = E_2 = 2 \cdot 10^9$ N/m^2, b = 0.5 m^{-1}s.

3. NUMERICAL SIMULATIONS AND BIFURCATION DYNAMICS

During the presented in this section numerical simulations the following set of parameters remains constant: m_1=4.59 kg, m_2 = 2.41 kg, $I_{x1} = I_{y1}$ = 0.0315 kg·m^2, I_{z1} = 0.0078 kg·m^2, I_{x2} = 0.0084 kg·m^2, I_{y2} = 0.0055 kg·m^2, I_{z2} = 0.0038 kg·m^2, L_1 = 0.228 m, L_2 = 0.175 m, e_1 = 0.122 m, e_2 = 0.0586 m, R_b = 0.025 m, g = 9.81 m/s^2, M_b = 0.04 N·m, ε_b = 0.4, b = 0.5 m^{-1}s, $\nu_1 = \nu_2$= 0.3, $E_1 = E_2 = 2 \cdot 10^9$ N/m^2, μ = 0.2, b_T = 0.681, $\varepsilon = 10^{-3}$.
In Figs. 3-9 one can observe results of numerical investigations of collision of the stable equilibrium position of the pendulum with the obstacle. The driving parameters of the pendulum are choosen in such a way, that for the parameter $z_0 < z_0^* = -L_1 - L_2 - R_b$, the system tends to the stable equilibrium position at $\theta_1 = \varphi_1 = \theta_2 = \varphi_2 = 0$. Displacement of the obstacle over the threshold z_0^* (playing a role of bifurcational parameter) leads to complex dynamical behavior and potentially rare/uknown bifurcation scenarios.
Figure 3 exhibits example of bifurcation scenario for the following driving parameters: $\omega_0 = 2\,\text{rad/s}$, $q = 6\,\text{rad/s}$, $\Omega = 2\,\text{rad/s}$ and for non-rotating disk of the obstacle ($\omega_d = 0$). After collision with the obstacle, the perioidc orbit appears (Fig. 3(b)), which then (after further growing of the horizintal poistion of the obstacle) transit into a quasiperidicity (Fig. 3(c-f, h-i)), with periodic windows (Fig. 3(g)). Further increase of bifurcational parameter z_0 allows to observe also chaotic motion (Fig.3(j, k)).

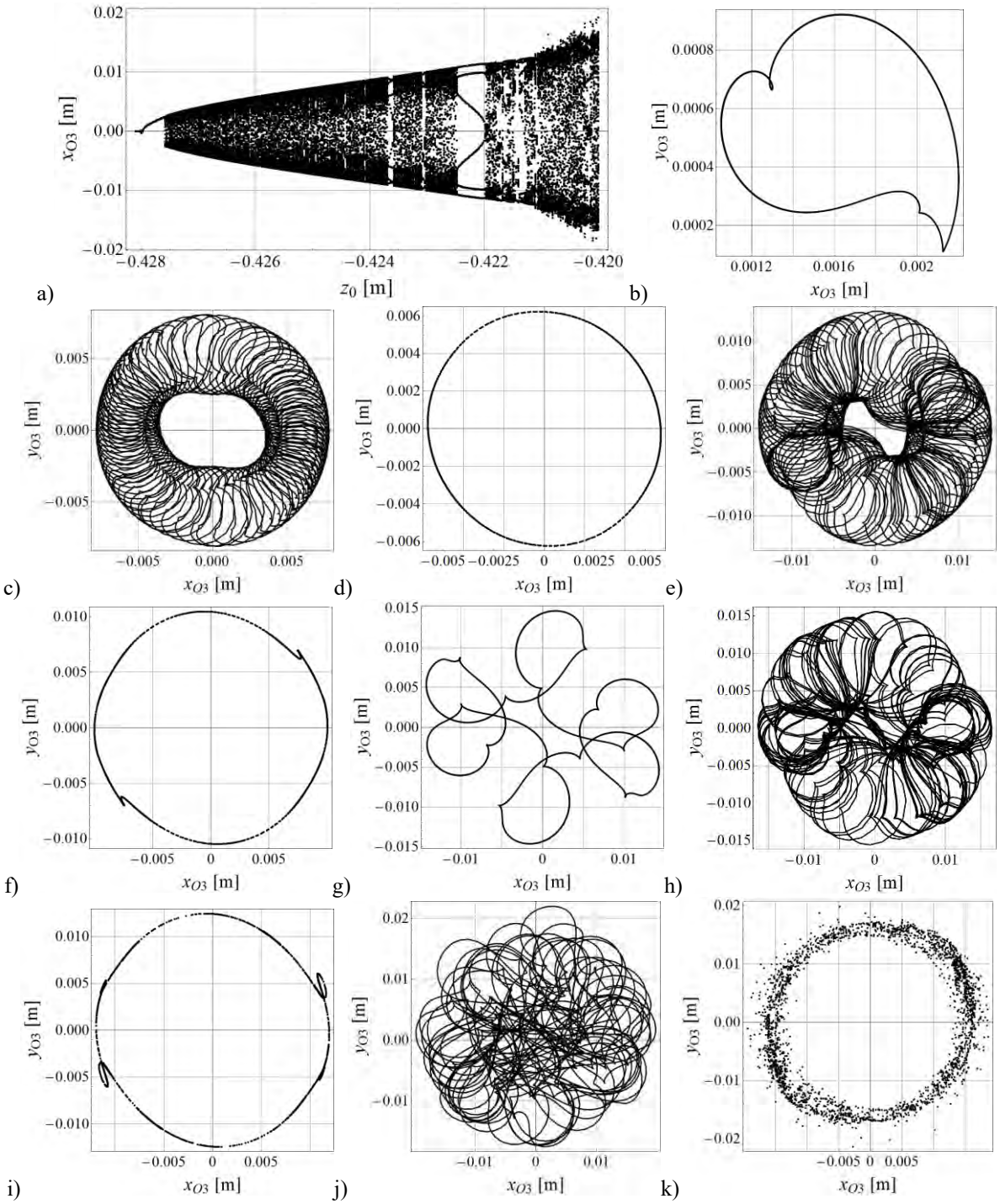

Figure 3. Bifurcation diagram of the system ($\omega_0 = 2\,\text{rad/s}$, $q = 6\,\text{rad/s}$, $\Omega = 2\,\text{rad/s}$, $\omega_d = 0$) (a) and the corresponding attractors for: $z_0 = -0.4278$ m - orbit (b), $z_0 = -0.426$ m - orbit (c) and Poincaré section (d), $z_0 = -0.423$ m - orbit (e) and Poincaré section (f), $z_0 = -0.4221$ m - orbit (g), $z_0 = -0.4215$ m - orbit (h) and Poincaré section (i), $z_0 = -0.42$ m - orbit (j) and Poincaré section (k).

Another scenario is presented in Fig. 4, where the previous settings of the driving are applied but the obtacle is now rotating with angular velocity $\omega_d = 10\,\text{rad/s}$. This change leads to sudden occurence of chaotic atttractor just after collision of the stable equlibrium position with the obstacle (see two examples of chaotic attractor in Fig.4(b-e)).

The following parameters of the driving: $\omega_0 = 0$, $q = 10\,\text{rad/s}$, $\Omega = 2\,\text{rad/s}$ and non-rotating obstacle ($\omega_d = 0$) leads to results presented in Fig. 5. In this case, similarly as in the example shown in Fig. 3, the periodic orbit occurs after the

collision with the disk (Fig. 5(b)), but then it transit directly to the chaotic region during further change of the parameter z_0 (see Fig. 5 (c-d)). For higher positions of the obstacle mainly perriodic attractor is observed (Fig 5(e)).
Further examples are presented in Figs. 6-9, where different driving parameters are applied. One can observe similar scenarios as shown prevously: sudden occurence of chaos (Fig. 6-8) and birth of periodic attractor, whcih then trasnsits to chaos (Fig. 9).

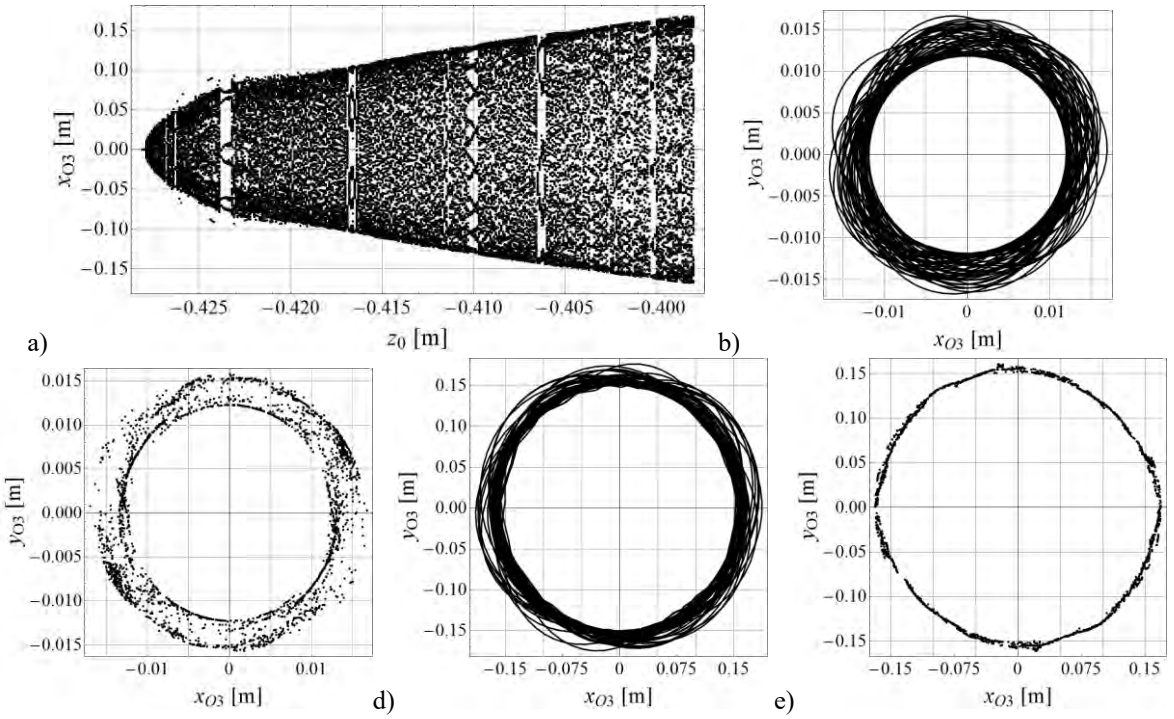

Figure 4. Bifurcation diagram of the system ($\omega_0 = 2\,\text{rad/s}$, $q = 6\,\text{rad/s}$, $\Omega = 2\,\text{rad/s}$, $\omega_d = 10\,\text{rad/s}$) (a) and the corresponding attractors for: $z_0 = -0.4278$ m - orbit (b) and Poincaré section (c), $z_0 = -0.398$m - orbit (d) and Poincaré section (e).

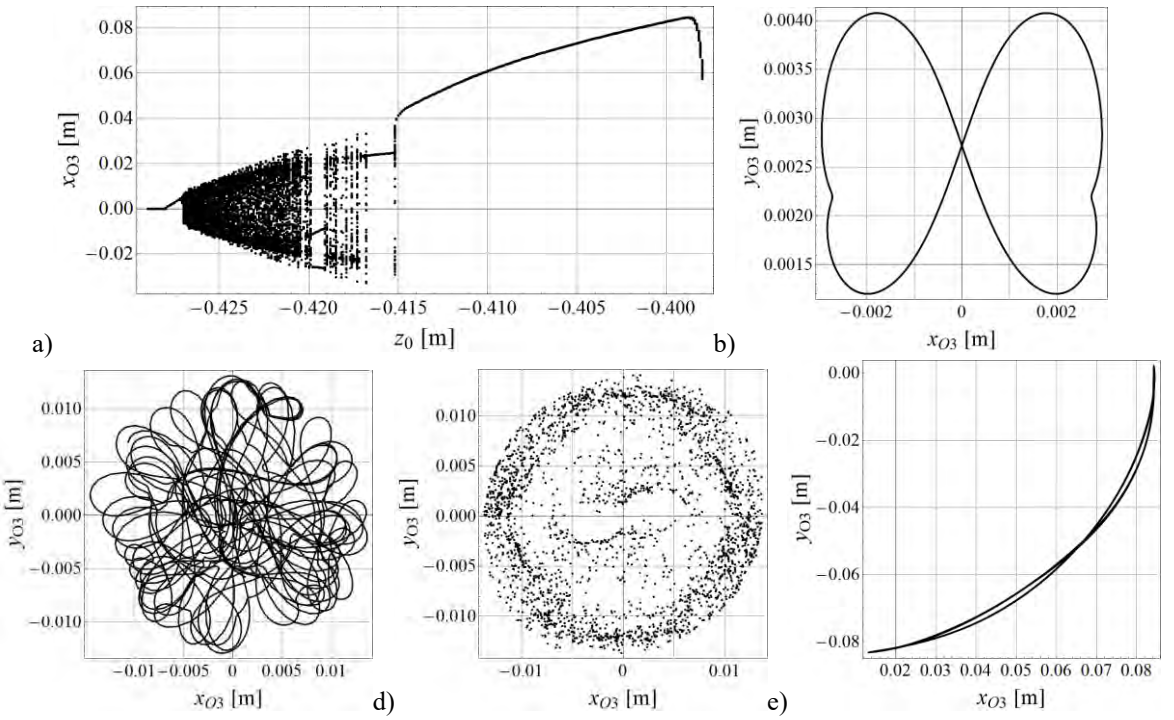

Figure 5. Bifurcation diagram of the system ($\omega_0 = 0$, $q = 10\,\text{rad/s}$, $\Omega = 2\,\text{rad/s}$, $\omega_d = 0$) (a) and the corresponding attractors for: $z_0 = -0.4275$m - orbit (b), $z_0 = -0.425$m - orbit (c) and Poincaré section (d), $z_0 = -0.440$m - orbit (e),

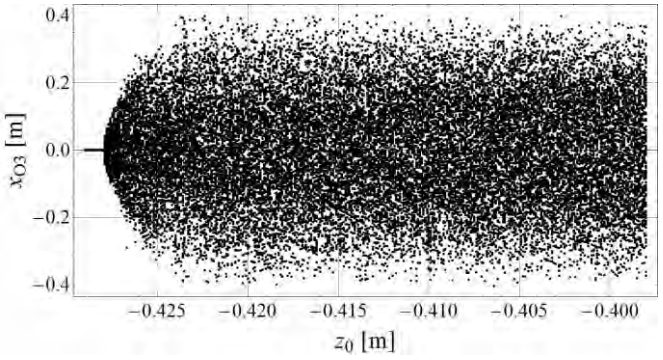

Figure 6. Bifurcation diagram of the system for the parameters: $\omega_0 = 0\,\text{rad/s}$, $q = 10\,\text{rad/s}$, $\Omega = 2\,\text{rad/s}$, $\omega_d = 50\,\text{rad/s}$.

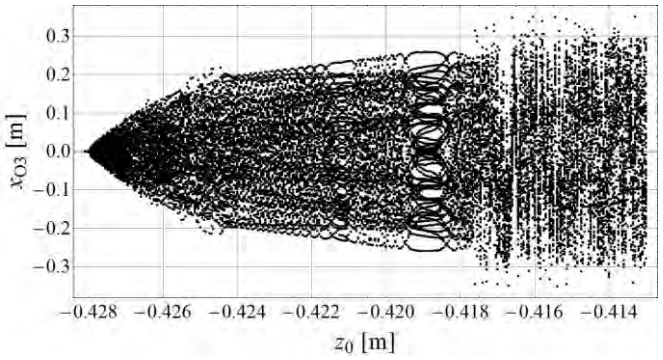

Figure 7. Bifurcation diagram of the system for the parameters: $\omega_0 = 5\,\text{rad/s}$, $q = 2\,\text{rad/s}$, $\Omega = 6\,\text{rad/s}$, $\omega_d = -10\,\text{rad/s}$.

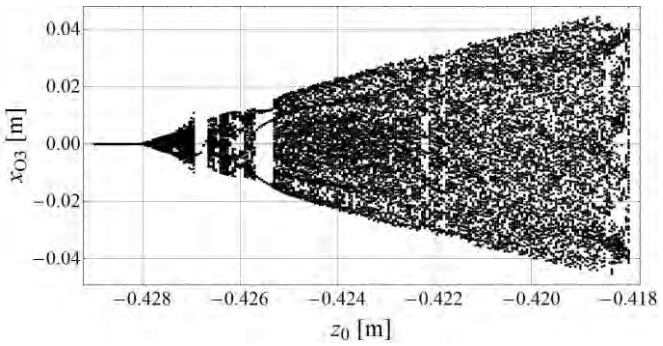

Figure 8. Bifurcation diagram of the system for the parameters: $\omega_0 = 0\,\text{rad/s}$, $q = 10\,\text{rad/s}$, $\Omega = 3\,\text{rad/s}$, $\omega_d = -5\,\text{rad/s}$.

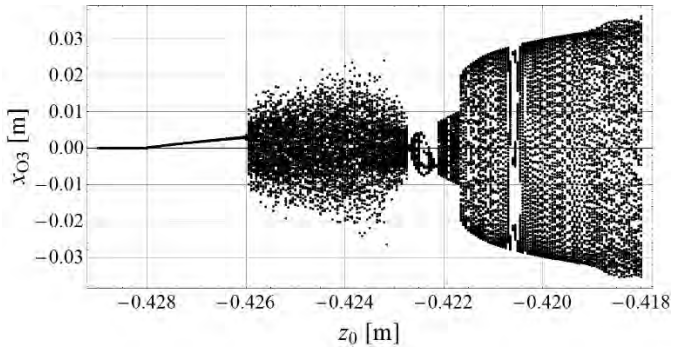

Figure 9. Bifurcation diagram of the system for the parameters: $\omega_0 = 0\,\text{rad/s}$, $q = 5\,\text{rad/s}$, $\Omega = 3\,\text{rad/s}$, $\omega_d = -5\,\text{rad/s}$.

4. CONLUDING REMARKS

The work present, probably for the first time in the literature, application of special class of reduced models of resultant friction force based on Padé approximants and their extensions [9] in the modelling of impacts between two rigid bodies in 3D space. During the modelling some elements, e.g rolling resistance and friction torque, are neglected. We expect that their influence on the system behaviour is not essential, however it can be examined in the further investigations.

In should be noted that the paper exhibits preliminary results, being a stage of preparation before experimental invesigations of the experimental rig beeing under construction. There are shown a few types of bifurcation scnenarios related to collision of stable equilibrium position with rigid obstable, e.g: occurence of stable periodic orbit further undergoing transition to quasiperiodicity, birth of periodic attractor undergoing then transition to chaos or sudden transition to chaos just after the collision. This is not sistematic classification of the dynamic scnenarios and further detailed analysis is required. However, the presented examples concern situations, which are rather rare or not present in the scientific literature, thus one can expect to find new kinds of bifurcations.

ACKNOWLEDGEMENTS

This work has been supported by the Polish National Science Centre, MAESTRO 2, No. 2012/04/A/ST8/00738.

5. REFERENCES

[1] Shen, J., Sanyal, A.K., Chaturvedi, N.A., Bernstein, D., McClamroch, H. ,“Dynamics and control of a 3D pendulum” 43rd IEEE Conference on Decision and Control, Georgia, USA, December 2004, pp. 323–328.

[2] Chaturvedi, N.A., McClamroch, N.H. , “Asymptotic stabilization of the hanging equilibrium manifold of the 3D pendulum” International Journal of Robust and Nonlinear Control, 17(16), 2007, pp. 1435–1454.

[3] Chaturvedi, N.A. , Lee, T. , Leok, M., McClamroch, N.H., “Nonlinear Dynamics of the 3D Pendulum” Journal of Nonlinear Science, 21(1), 2010, pp. 3–32.

[4] Náprstek, J., Fischer, C.,“Types and stability of quasi-periodic response of a spherical pendulum”, Computers & Structures, 124, 2013, pp. 74–87.

[5] Ludwicki, M., Awrejcewicz, J., Kudra, G., „Spatial double physical pendulum with axial excitation: computer simulation and experimental set-up” International Journal of Dynamics and Control, *3*(1), 2015, 1–8. http://doi.org/10.1007/s40435-014-0073-x.

[6] Contensou, P., 1963, “Couplage entre frottement de glissement et de pivotement dans la téorie de la toupe”, In: Ziegler H. (Ed.), Kreiselprobleme Gyrodynamic, IUTAM Symposium Celerina, Springer-Verlag, Berlin, 1962, pp. 201-216.

[7] Zhuravlev, V.P., “The model of dry friction in the problem of the rolling of rigid bodies”, Journal of Applied Mathematics and Mechanics, 62(5), 1998, pp. 705-710.

[8] Zhuravlev V. P., Kireenkov A.A., “Padé expansions in the two-dimensional model of Coulomb friction”, Mechanics of Solids 40(2), 2005 1-10.

[9] Kudra, G., Awrejcewicz, J., “Approximate modelling of resulting dry friction forces and rolling resistance for elliptic contact shape”, European Journal of Mechanics A/Solids, 42, 2013, pp. 358-375.

[10] Kudra, G., Awrejcewicz, J., “Application and experimental validation of new computational models of friction forces and rolling resistance”, Acta Mechanica, 226(9) (2015), 2831-2848.

[11] Kudra, G., Szewc, M., Wojtunik, I., Awrejcewicz, J., „Shaping the trajectory of the billiard ball with approximations of the resultant contact forces”, Mechatronics, 37, 2016, pp. 54–62. http://doi.org/10.1016/j.mechatronics.2016.01.002.

[12] Kudra, G., Szewc, M., Wojtunik, I., Awrejcewicz, J., “On some approximations of the resultant contact forces and their application in rigid body dynamics”, Mechanical Systems and Signal Processing, 79, 2016, pp. 182–191.

[13] Gilardi, G., Sharf, I., “Literature survey of contact dynamics modelling. Mechanism and Machine Theory”, 37(10), 2012, pp.1213–1239. http://doi.org/10.1016/S0094-114X(02)00045-9.

[14] Hunt, K.H., Crossley, F.R.E., “Coefficient of restitution interpreted as damping in vibroimpact”, Journal of Applied Mechanics, 42, Series E, 1975, pp. 440–445.